SLAC–PUB–5524
July 1991
(E)

SEARCH FOR MINIMAL SUPERSYMMETRIC MODEL HIGGS WITH SLD*

JI MA
Stanford Linear Accelerator Center
Stanford University, Stanford CA 94309

Abstract

This report presents results from a Monte Carlo study on the possibility of searching for the Minimal Supersymmetric Model Higgs bosons using the SLD detector and the SLC. The primary results show that with 8 K hadronic Z^0 events, one should be able to search the as yet unexplored area in m_{h^0}, m_A parameter space. The study indicates that superior calorimetry and vertex detection are crucial for such a Higgs search. This investigation has been done with JETSET (Version 6.3) of the Lund Monte Carlo program.

1. Introduction

Spontaneous symmetry breaking is the foundation of the Standard Model (SM) of the electromagnetic and weak interactions. In local gauge invariant theories, spontaneous symmetry breaking requires the existence of one or more scalar particles, called Higgs bosons. However, while the SM has been successful in describing many processes to a high degree of accuracy, these scalar particles have not been observed. There are problems such as fine-tuning, naturalness, and hierarchy that the SM can not answer by itself. A calculation of the first order correction to the Higgs boson mass squared yields a quadratically divergent correction arising from SM particle loop graphs. Several different ways of regulating the divergence have been proposed including supersymmetry and technicolor. Here we focus on the Minimal Supersymmetric Model (MSSM), a minimum extension of the SM, which contains two complex Higgs doublets. I briefly describe some aspects of the MSSM model. More detailed discussions can be found in "Higgs Hunter's Guide."[1]

In the MSSM model, one of the Higgs doublets H_1 couples to *down*-type of quarks and leptons, while the other doublet H_2 couples to *up*-type of quarks and leptons. This requirement prevents tree-level flavor-changing neutral currents. There are eight real fields for the two complex Higgs doublets. When the symmetry spontaneously breaks down, three of these fields are *eaten* by intermediate gauge bosons, and each gauge boson gains one more degree of freedom and becomes a massive particle. The remaining five fields become physical Higgs bosons that are classified as follows:

* Work supported by Department of Energy contract DE–AC03–76SF00515.

(1) Two charge Higgs bosons with mass greater than that of the W-boson.

(2) Two neutral CP-even Higgs bosons, one (h^0) must be lighter than the Z^0, while the other (H^0) must be heavier than the Z^0.

(3) One neutral CP-odd Higgs boson (A) which has to be heavier than the h^0, but can be lighter than the Z^0 and might therefore be accessible to experiments running near the Z^0 resonance.

Obviously only h^0 and/or A can be accessible at the SLC, which was designed to run at the energy of the Z^0 resonance.

2. Parameters

In the MSSM model, only two independent parameters (plus a sign) are needed to fully specify the Higgs sector (i.e., Higgs production and decay). These parameters can be chosen to be:

(1) $\tan\beta = v_2/v_1$, the ratio of vacuum expectation values of the Higgs doublets (where doublet 2 couples to up-type quarks and leptons, and doublet 1 couples only to down-types).

(2) m_{h^0}, the mass of the lightest Higgs boson (h^0).

Alternatively, one can chose:

(1) m_{h^0}, the mass of lightest Higgs boson (h^0).

(2) m_A, the mass of the CP-odd Higgs boson (A).

For a given choice of m_{h^0}, m_A there are two solutions, one for $\tan\beta > 1$ and one for $\tan\beta < 1$. Many models[1] favor $\tan\beta > 1$. My study concerns the $\tan\beta < 1$ case. The reasons are twofold. First, the $\tan\beta < 1$ case is much more difficult to detect than $\tan\beta > 1$, since both h^0 and A essentially decay only to $c\bar{c}$ which is difficult to tag. Those Higgs no longer decay leptonically; thus they are much more difficult for LEP detectors to detect. Second, if a method works for $\tan\beta < 1$ case, similar methods can be used to deal with the $\tan\beta > 1$ case.

3. Current Search Limits

Mass limits currently show that the region where the sum of the h^0 and A Higgs masses are close to the mass of Z^0 still has not been explored for either $\tan\beta < 1$ or $\tan\beta > 1$. See the shaded region of Fig. 1. In the most recent report on the MSSM Higgs search,[2] limits have been set that exclude the white region of Fig. 1.

4. Higgs Production

MSSM Higgs with masses below the Z^0 mass can be produced from one of the two Z^0 decay modes:

Production Mode	Partial Width	Limits ($m_{h^0} \to m_A$)
$Z^0 \to h^0 Z^*$	$\frac{\Gamma(Z \to h^0 Z^*)}{\Gamma(Z \to H Z^*)} = \sin^2(\beta - \alpha)$	$\to 0$
$Z^0 \to h^0 A$	$\frac{\Gamma(Z \to h^0 A)}{\Gamma(Z \to \nu_e \bar{\nu}_e)} = \frac{1}{2} \cos^2(\beta - \alpha)\ B^{3/2}$	$\to B^{3/2}$

Here H is the standard model Higgs, and $B = 2|P|/m_Z$; $|P|$ is the magnitude of the final Higgs momentum. The limits for the first channel can be inferred from a conventional Higgs search, since its partial decay width is proportional to that of Standard Model Higgs (see table above). The dashed line labeled $Z^0 \to hZ^{0*}$ is the limit set by using the first channel. We can see that this limit is always off the diagonal line, since when $m_{h^0} \to m_A$, $\sin^2(\beta - \alpha) \to 0$ the branching ratio goes to zero on the diagonal line (see limits in above table). On other hand, the second channel is enhanced as $m_{h^0} \to m_A$; see Fig. 1. The fine dotted line corresponds to the limits set by using the second mode. Notice that this mode only covers the region near the diagonal line where the partial width reaches maximum (see limits in the above table). The same conclusion is true for the unexplored region (shaded region), except that the branching ratio is even smaller; (see Fig. 2). Thus the second channel is the dominant mode in our region of interest.

5. Higgs Decay

A general feature of the MSSM Higgs' couplings with quarks and leptons is that the couplings are proportional to the mass of the quark or lepton and some *angle factor* (α, β). This implies that Higgs bosons tend to decay to the heaviest quark or lepton kinematically accessible if it is not suppressed by the angle factors.

The angle factors for the couplings of all Higgs production and decay modes are plotted in Fig. 3 ($m_A = 30GeV, \tan\beta < 1$). The general features are:

(1) The two Higgs production modes are complementary, the first being large when the second is small and vice versa.

(2) For $\tan\beta > 1$, the two Higgs tend to decay to *down*-type fermions.

(3) For $\tan\beta < 1$, the two Higgs tend to decay to *up*-type fermions.

Specifically, in our region of interest, for $m_{h^0} = 40$ GeV, $m_A = 45$ GeV, MSSM predicts the following:

$$\begin{aligned} \tan\beta > 1 \quad & h^0,\ A \to b\bar{b}\ (\approx 93\%)\ , \quad \tau^+\tau^-\ (\approx 6\%) \\ \tan\beta < 1 \quad & h^0,\ A \to c\bar{c}\ (\approx 97\%)\ , \quad b\bar{b}\ (\approx 3\%)\ . \end{aligned}$$

Notice that for $\tan\beta > 1$, there is always a significant leptonic channel which can be utilized if there are enough events. But for $\tan\beta < 1$, there is no leptonic channel—only the heavy quark channels are available. This means the heavy quark has to be tagged in order for the Higgs to be seen. This would be very difficult without good calorimetry and vertex detection. These two parts of the detector are crucial in our Higgs-hunting game.

Obviously, the only possible channels that can be used in this case is

$$Z^0 \to h^0 A \to c\bar{c}c\bar{c};\ b\bar{b}c\bar{c};\ b\bar{b}b\bar{b}$$

with Higgs-to-background ($Z^0 \to$ hadrons) ratio of 1:207. Thus our Higgs final state is a 4c-jet state embedded in a large Z^0 QCD background. The QCD $Z^0 \to c\bar{c}c\bar{c}$ decay is extremely rare (26 events per 10 K Z^0 decays). These events are also included in our background samples.

6. Hunting Strategy

The following chart summarizes all Z^0 decay channels, except the invisible modes, and various methods of eliminating the backgrounds. We omit discussion of leptonic backgrounds since these events have distinct signatures. The charge multiplicities for leptonic events are much lower than for their hadronic counterpart, and are easily identified.

Z^0(10 K)	$l\bar{l}$	2640	Clear signature
	$u\bar{u} + d\bar{d} + s\bar{s}$	3970	Vertex track fit
	$c\bar{c}$	1110	4-jet cut
	$b\bar{b}$	1430	4-jet cut
	Higgs	53	E, P balance Invariant mass

6.1 The jet reconstruction

A jet is defined as a collimated collection of particles formed in high energy particle interactions. When very heavy particles decay into quarks, the secondary particles usually form jets.

For jet reconstruction, we use the CERN LUCLUS routine. The LUCLUS sorts the track sample into two groups. Particles with momentum greater than $P_{cut} = 0.25GeV$ are in one group and the rest are in another. The program starts with the large momentum group, from which it selects the most energetic particle. It then calculates *distance* between the fastest particle and rest of the particles in the large momentum group.

The *distance* is defined as follows:

$$d_{ij} = \sqrt{(P_i P_j - \vec{P}_i \cdot \vec{P}_j) \frac{2P_i P_j}{(P_i + P_j)^2}} = \sqrt{(1 - \cos\theta_{ij}) \frac{2(P_i P_j)^2}{(P_i + P_j)^2}},$$

where P_i, P_j are the momentum for the ith and jth particles, and θ_{ij} is the angle between them. The *distance* reduces to the transverse momentum when the magnitude of one of the momenta is much larger than the other, and to half of the transverse momentum when the two momenta are of the same magnitude.

Those particles whose *distance* is less than P_{cut} are merged with the fastest particle. The fastest particle plus the merged particles become a core for one jet. The program repeats this process on the remaining particles in the large momentum group until all particles are used up. Thus the large momentum group particles are partitioned into one-to-several jet cores.

Next the program attaches small momentum particles to the nearest jet, with a symmetric *distance* measure between particle and jet. Finally, it checks whether any two jets are within the specified jet resolution power d_{join} (the *distance* between two jets) and combines these jets whose *distance* are less the d_{join}.

Our channel of interest has two Higgs bosons, both of which decay into $c\bar{c}$ quark pairs. When the $c\bar{c}$ pairs hadronize, charmed mesons or baryons then form 4-jet events. Therefore we select only 4-jet events as our Higgs sample. The selection efficiency is defined as the ratio of the number of events which pass the 4-jet cut and the total number of generated events. We need to tune the jet finder (jet resolution power) to filter out background events while retaining most Higgs events. Figure 4 shows the selection efficiency versus jet resolution power for all background and Higgs events. The selection efficiency for background events drops quickly as d_{join} increases. For the Higgs events, the selection efficiency decreases very slowly as we increase d_{join}, since a Higgs event is a true 4-jet event. We chose the jet resolution power to be $d_{\text{join}} = 3.25$ GeV.

After this 4-jet cut, the background is reduced by one order of magnitude.

Event Type	Samples	4-Jet Cut	Pass (%)
$u\bar{u} + d\bar{d} + s\bar{s}$	3970	670	16.9
$c\bar{c}$	1110	148	13.3
$b\bar{b}$	1430	174	12.2
Higgs	53	45	84.9

6.2 Vertex fitting

SLD is equipped with a high-precision vertex detector which helps heavy quark tagging. In a light quark event, the mesons produced from the light quark have a long lifetime and do not decay inside the vertex chamber. Therefore, essentially all tracks come from the primary interaction point. On the other hand, heavy quarks hadronized into hadrons that travel for a short distance from the primary interaction point and then decay into secondary particles. Thus, in principle, one only needs to count how many secondary and primary tracks are being seen inside the vertex chamber to separate the heavy quark events from light quark events. It turns out that this method works for the events in which heavy quarks are energetic, hence the decay point of heavy hadrons are significantly away from the primary interaction point. In Higgs events, where $Z^0 \rightarrow h^0 A \rightarrow c\bar{c}c\bar{c}$, each heavy meson travels less than half the distance before decaying than those formed in $Z^0 \rightarrow c\bar{c}$ events do. This presents a difficulty for our secondary track finder, which designates half of secondary tracks to be primary tracks. Hence the number of secondary tracks in the Higgs events is not very different from that of u.d.s events.

A more successful approach is to fit all the tracks measured in the vertex chamber to a single primary interaction point. Figure 5 shows the Monte Carlo simulation of a primary vertex fit for various samples. Light quark events always give a good fit (plot A) and heavy quark events generally give a poor fit (plots B, C, D). The r.m.s. distribution for $c\bar{c}$ is broad, and for $b\bar{b}$ is even broader, since bottom mesons have two sequential short-lived decays. The Higgs events have a very broad r.m.s. distribution because there are a large number of low-energy secondary particles being used to fit the primary vertex, and those low-energy secondary particles have larger impact parameters. A cut on r.m.s. is made to get rid of most of u.d.s. and part of $c\bar{c}$, $b\bar{b}$. The result is:

Event Type	4-Jet Cut	Primary Vertex Fi	Pass (%)
$u\bar{u} + d\bar{d} + s\bar{s}$	670	139	20.7
$c\bar{c}$	148	76	51.4
$b\bar{b}$	174	155	89.1
Higgs	45	38	84.4

6.3 Energy momentum balance

In order to obtain a better Higgs invariant mass plot, we need to have an accurate jet momentum and energy measurement. Missing energy is the common problem in any energy measurement. It can be due to neutrinos escaping the detector, dead regions of the detector, or albedo. Since detector response to hadronic showers is different than its response to electromagnetic showers (the so-called e/π ratio), there is a large visible energy fluctuation in the calorimeter energy measurement. A poor energy, and thus momentum, measurement means a broad invariant mass resolution for the Higgs particles, which makes signal and background separation more difficult. For our 4-jet system, the following technique can significantly remove these effects.

The total energy and momentum of the interaction are known, which provides a very strong constraint on our measured jet 4-momenta. We use them to make corrections to our jet 4-momentum.

Since the invariant mass of each jet (a few GeV) is quite small compared to its energy and momentum ($\approx$ 20 GeV), the energy and momentum of a jet are almost equal. Hence, to a good approximation, they can be corrected by the same factor.

Let $(C_i|\ i = 1,2,3,4)$ be the factor needed to correct energy and momentum of jets number 1, 2, 3, 4. Then we have the following equations:

$$\begin{aligned} P_x^1 C_1 + P_x^2 C_2 + P_x^3 C_3 + P_x^4 C_4 &= 0 \\ P_y^1 C_1 + P_y^2 C_2 + P_y^3 C_3 + P_y^4 C_4 &= 0 \\ P_z^1 C_1 + P_z^2 C_2 + P_z^3 C_3 + P_z^4 C_4 &= 0 \\ E^1 C_1 + E^2 C_2 + E^3 C_3 + E^4 C_4 &= m_{z0}\ . \end{aligned}$$

This set of equations can be easily solved. The corrected energy and momentum are:

$$p'^i_\mu = C_i * p^i_\mu\ ; \quad i = 1,2,3,4\ ,$$

where p'^i_μ is the 4-momentum vector after correction and C_i is the multiplication factor for the ith jet.

Figure 6 shows the 4-jet invariant mass spectrum before (a) and after (b) the E, P balance correction. Without the energy-momentum constraint, it is very difficult to resolve a mass peak from the background. However, we still need good energy-momentum resolution to start with for this technique to work.

6.4 Reconstruction of Higgs mass

Each event is resolved into 4-jets. The invariant masses of the correct two-jet pairing give the masses of two Higgs particles. Since we don't know

which pair is the right one, we group all possible pairs and calculate the invariant pair mass. The smaller mass is plotted on one axes and the larger one on the other. The right pairing will always fall at the same point (crossing point of the two Higgs masses) on the mass scatter plot, while the wrong pairs will spread all over (see Fig. 7d). The invariant mass of a two-jet-pair for background events does not corresponds to any intermediate particle state and thus the scatter plot for those background events forms a slowly varying surface (see Fig. 7a,b,c). The background events and the wrong pairings in the Higgs events contribute the background under the Higgs peak.

For each 4-jet event, there are three ways to pair up the jets; three entries per event for the invariant pair mass scatter plot. A cut can be made surrounding the resonance peak on $m_{h^0} m_A$ parameter space as follows:

$$(m_A - 45)^2 + (m_{h^0} - 40)^2 < 5 \ .$$

After this cut (see Fig. 6), we are left with:

Event Type	Primary Vertex Fit	Invariant Mass Cut	Pass (%)
$u\bar{u} + d\bar{d} + s\bar{s}$	139	16	11.5
$c\bar{c}$	76	17	22.4
$b\bar{b}$	155	22	14.2
Higgs	38	32	84.2

A rough estimate of the statistical significance of signal over background contamination shows

$$\frac{\text{Higgs}}{\sqrt{\text{Background}}} = \frac{32}{\sqrt{55}} = 4.3 \ .$$

This means our Higgs peak will be 4.3 times higher than the background standard deviation if there were MSSM Higgs events present. A more precise analysis would require a global fit to the signal and background, using a maximum likelihood technique. This technique should improve the signal significance.

7. Conclusions

From this Monte Carlo study, with approximately 10 K Z^0, we may be able to explore the final hunting ground of MSSM Higgs accessible from the Z^0. The superior calorimeter energy measurements and vertex finding of SLD are the most important tools in our Higgs search.

Acknowledgment

This project is under the supervision of Professor Paul Mockett. I would like to thank him for many constructive suggestions and comments he made during this study.

Reference

1. J. F. Gunion, H. E. Haber, G. L. Kane, and S. Dawson, "The Higgs Hunter's Guide," SCIPP-89/13, 404 (1989).

2. B. Adeva et al., for the L3 Collaboration, "Search for the Neutral Higgs Bosons of the Minimal Supersymmetric Standard Model from Z^0 Decays," Phys. Lett. **B251**, 311-320 (1990); CERN preprint L3-015.

Figure Captions

1. Current MSSM Higgs search limits. The shaded regions have not yet been excluded.

2. Branching Ratio for various Higgs masses.

3. *Angular Factors* for the couplings of Higgs production and decay.

4. Selection efficiency versus *jet resolution power* for all samples.

5. The r.m.s. of the primary interaction fit using all vertex tracks.

6. Four-momentum balance correction for invariant Higgs mass: (a) before, and (b) after.

7. The scatter plot of two invariant Higgs masses: (a) uds, (b) $c\bar{c}$, (c) $b\bar{b}$, (d) MSSM Higgs.

8. The scatter plot of two invariant masses for Higgs and background. Shaded columns are Higgs peak.

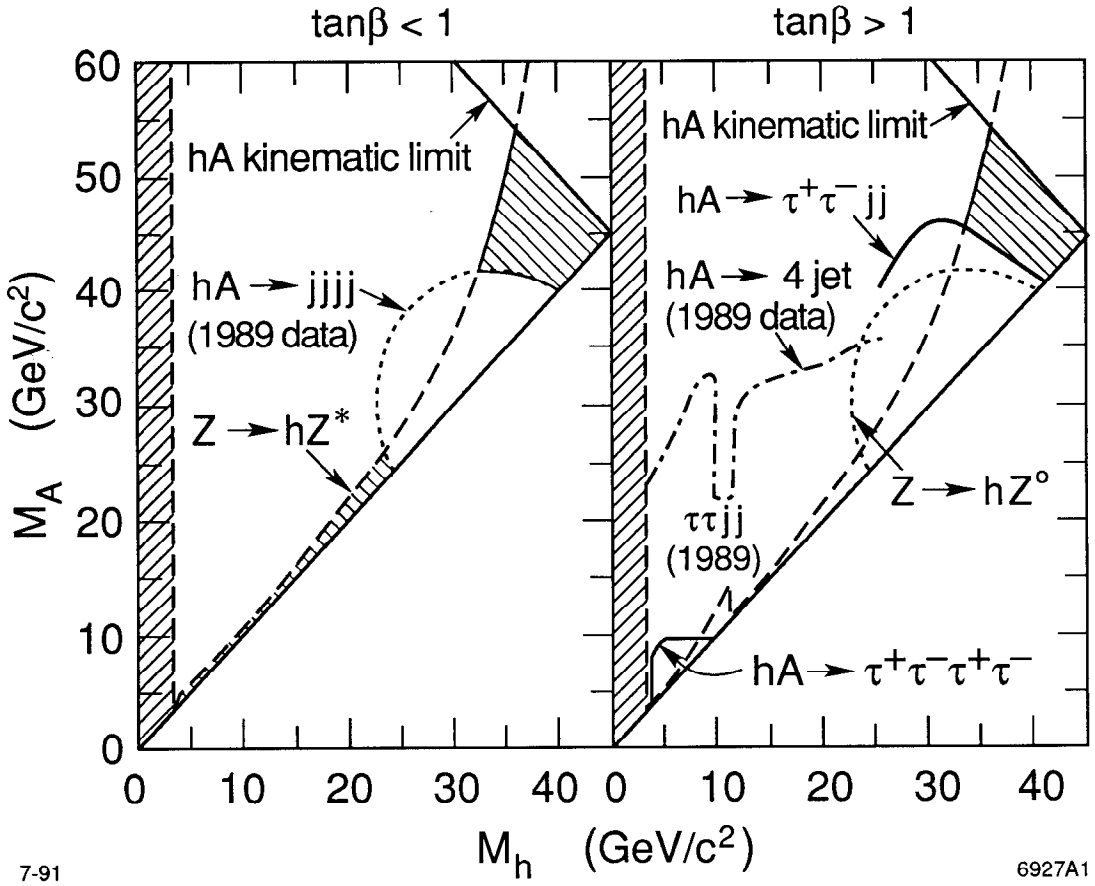
tanβ < 1
tanβ > 1
hA kinematic limit
hA → jjjj
(1989 data)
Z → hZ*
hA kinematic limit
hA → τ+τ− jj
hA → 4 jet
(1989 data)
Z → hZ°
ττjj
(1989)
hA → τ+τ−τ+τ−
MA (GeV/c2)
Mh (GeV/c2)
0
10
20
30
40
50
60
7-91
6927A1

Fig. 1

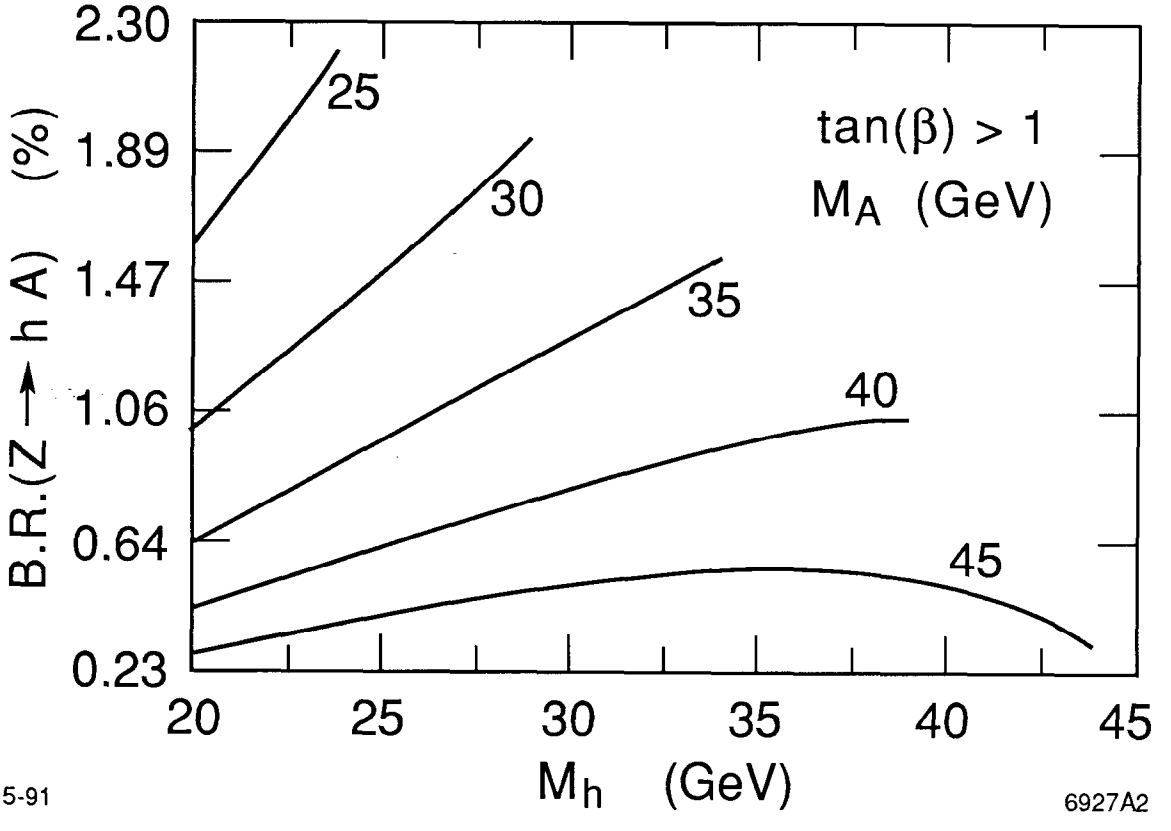
2.30
1.89
1.47
1.06
0.64
0.23
B.R.(Z → h A) (%)
25
30
35
40
45
tan(β) > 1
M_A (GeV)
20
25
30
35
40
45
M_h (GeV)
5-91
6927A2

Fig. 2

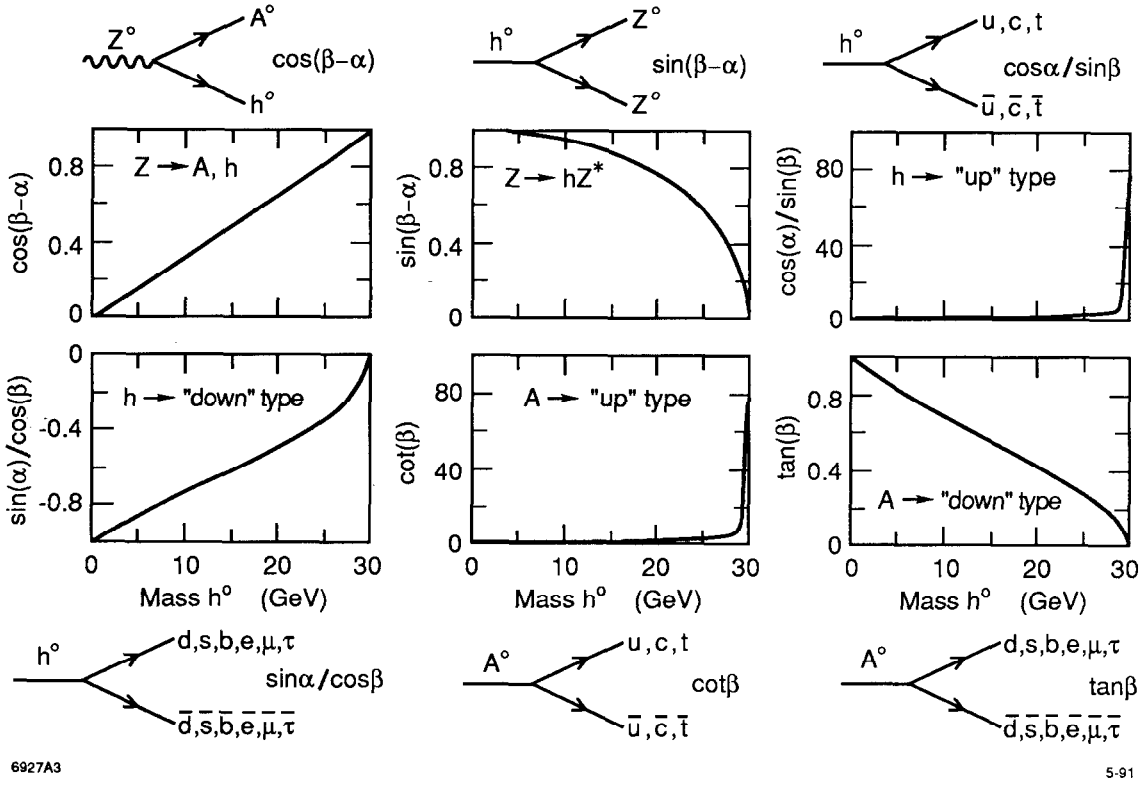
Z° A° h° cos(β−α)
h° Z° Z° sin(β−α)
h° u,c,t ū,c̄,t̄ cosα/sinβ
cos(β−α) 0.8 0.4 0 Z → A, h
sin(β−α) 0.8 0.4 0 Z → hZ*
cos(α)/sin(β) 80 40 0 h → "up" type
sin(α)/cos(β) 0 -0.4 -0.8 h → "down" type
cot(β) 80 40 0 A → "up" type
tan(β) 0.8 0.4 0 A → "down" type
0 10 20 30 Mass h° (GeV)
h° d,s,b,e,μ,τ d̄,s̄,b̄,ē,μ̄,τ̄ sinα/cosβ
A° u,c,t ū,c̄,t̄ cotβ
A° d,s,b,e,μ,τ d̄,s̄,b̄,ē,μ̄,τ̄ tanβ
6927A3
5-91

Fig. 3

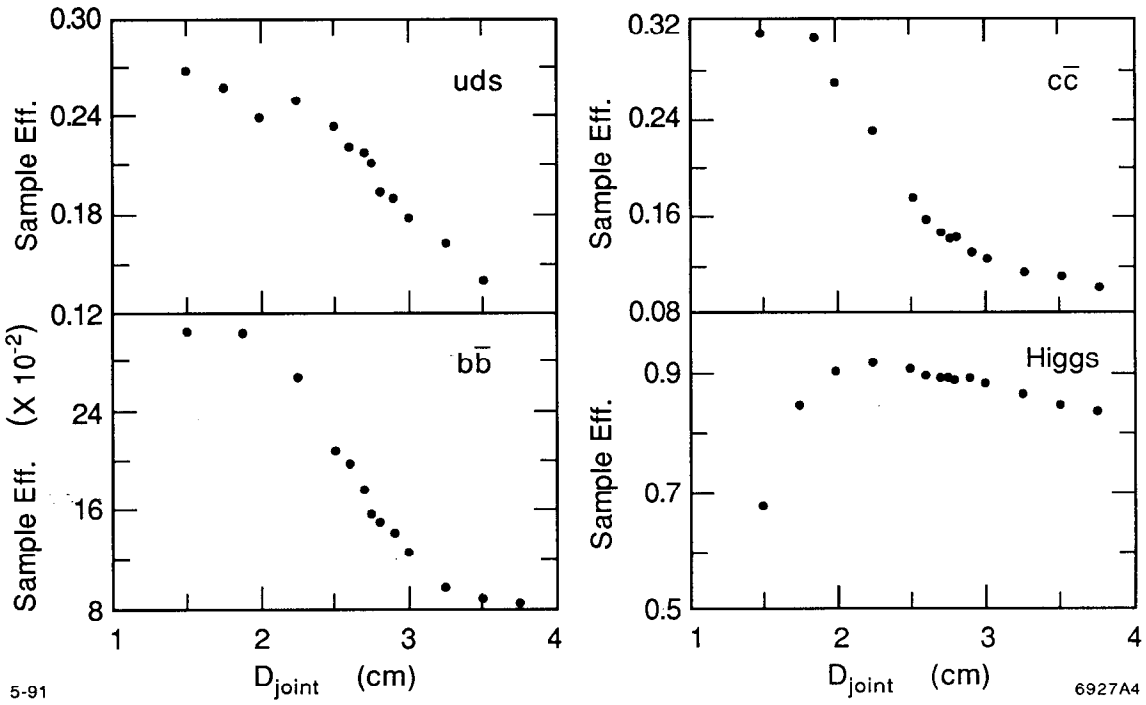
0.30
0.24
0.18
0.12
Sample Eff.
uds
Sample Eff. (X 10^{-2})
24
16
8
$b\bar{b}$
1
2
3
4
D_{joint} (cm)
5-91
0.32
0.24
0.16
0.08
Sample Eff.
$c\bar{c}$
0.9
0.7
0.5
Higgs
1
2
3
4
D_{joint} (cm)
6927A4

Fig. 4

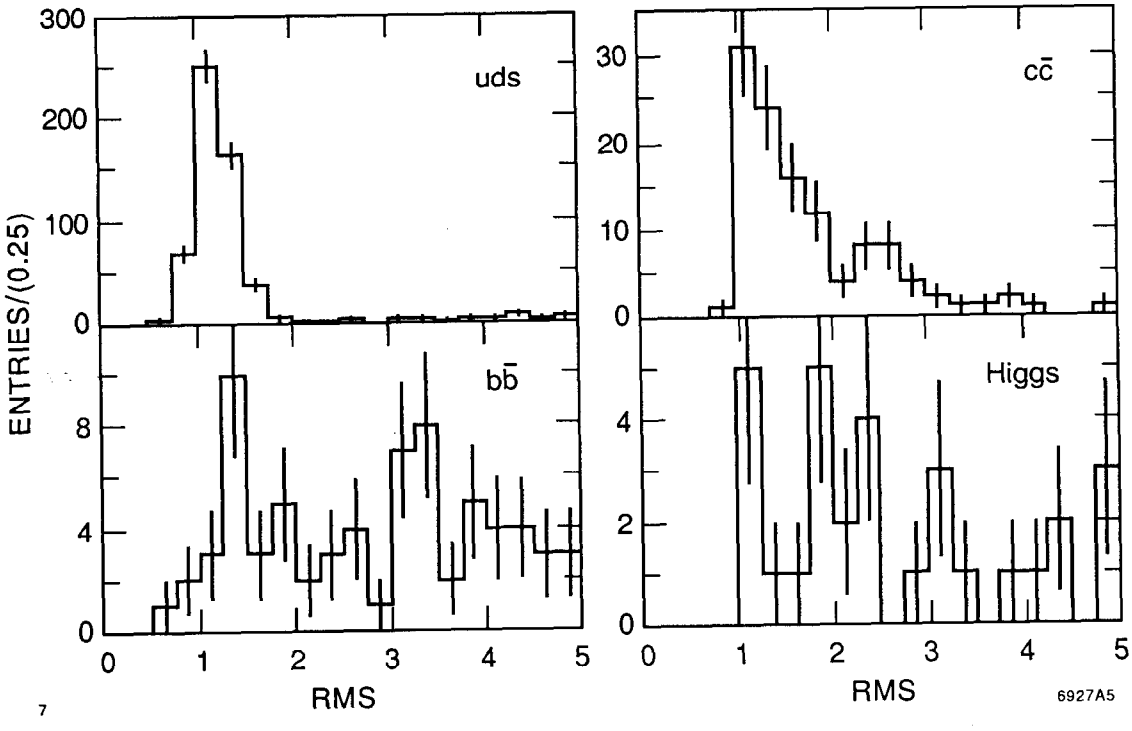

7-91

Fig. 5

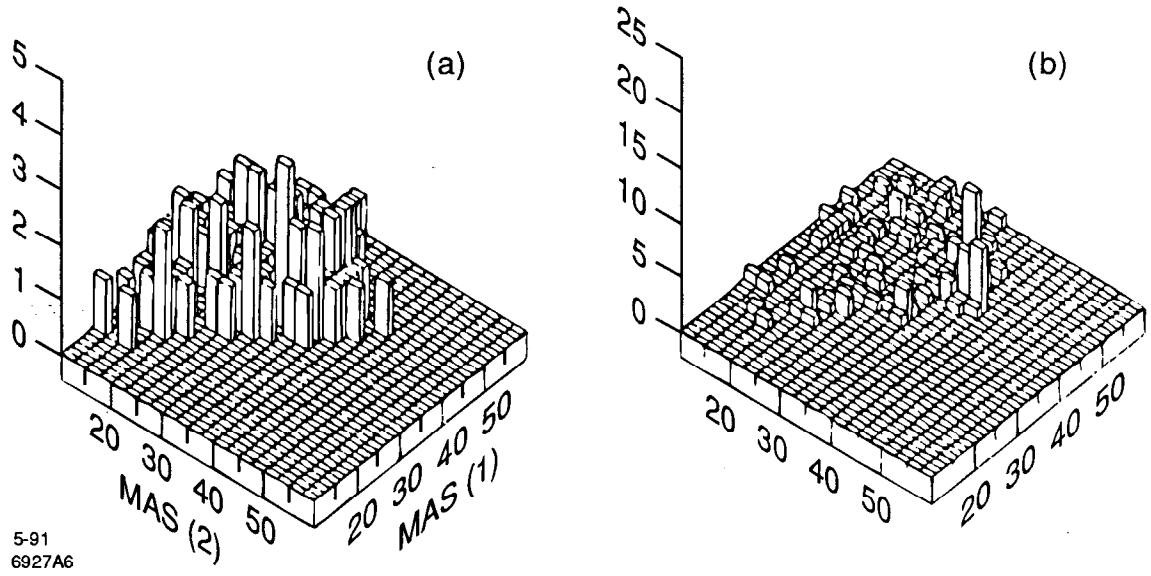
(a)
5
4
3
2
1
0
20
30
40
50
MAS (2)
20
30
40
50
MAS (1)
5-91
6927A6
(b)
25
20
15
10
5
0
20
30
40
50
20
30
40
50

Fig. 6

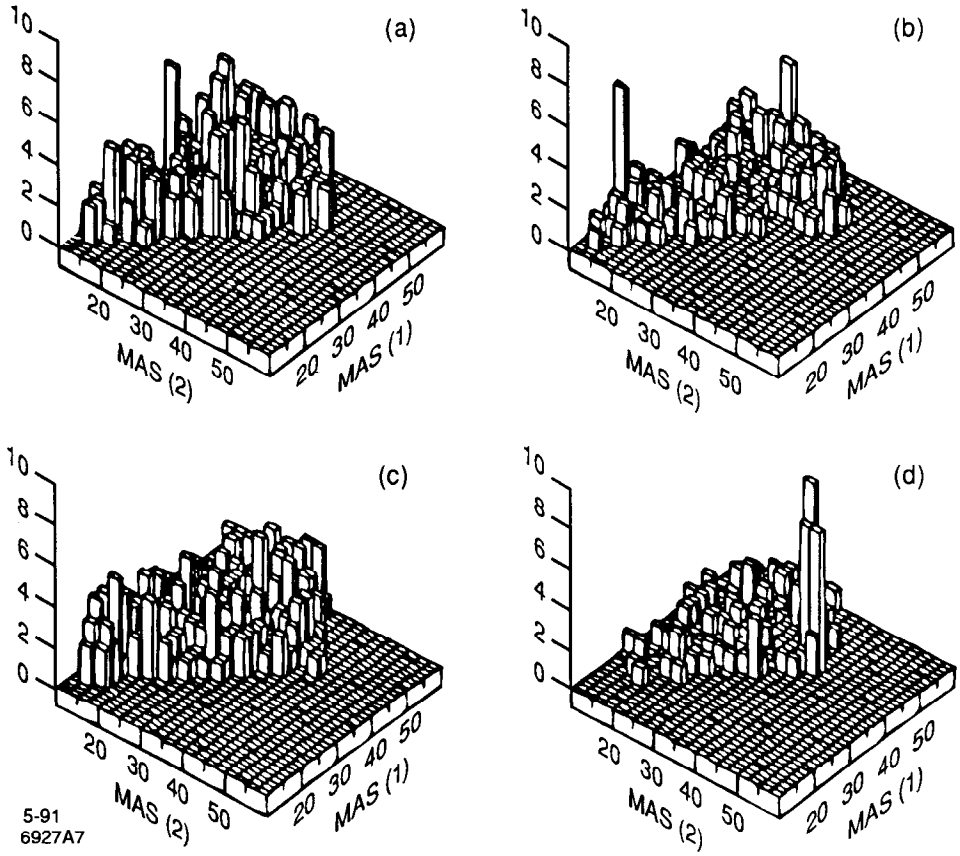

Fig. 7

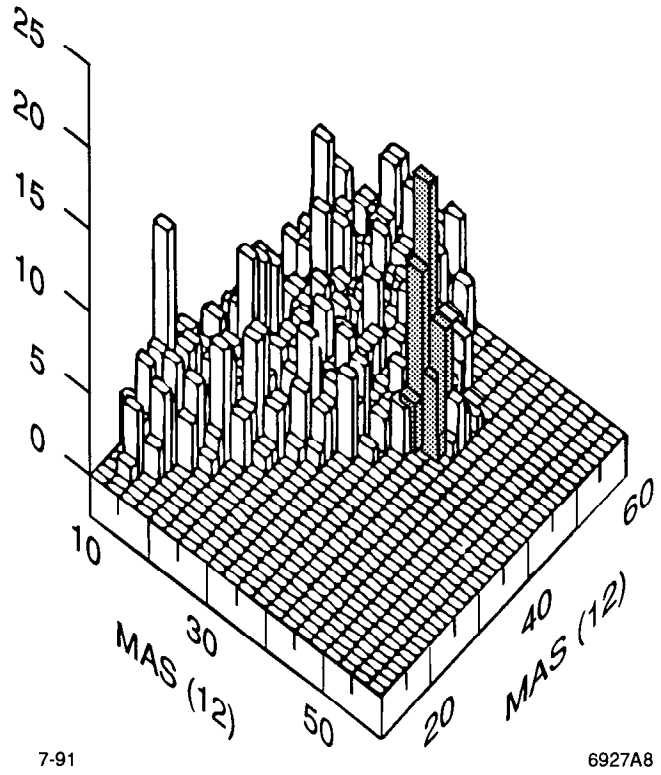

Fig. 8